A minimalist Stair Climbing Robot (SCR) formed as a leg balancing & climbing Mobile Inverted Pendulum (MIP)

Daniel Yang, Thomas Bewley, *UCSD Coordinated Robotics Lab*[1]

***Abstract*— This paper presents a (patent-pending) small, quasi-static, minimal-complexity Stair Climbing Robot (SCR). The vehicle design is given simply by adding a third motor to a (Segway-like) Mobile Inverted Pendulum (MIP), enabling it to maneuver up stairs, leveraging feedback control, by planting it's "foot" onto the ground in front of the next step, lifting the chassis/wheel assembly up it's own "leg", leaning over onto the top of the next step, self uprighting, and repeating for the following step(s). Fore/aft stabilization during leg balancing is given by using the MIP drive wheels as reaction wheels, while left/right stability is given by the width of the foot itself. The design is small and simple enough to potentially be ruggedized as a stair-climbing throwbot, akin to the Recon Scout (but able to climb up stairs) for reconnaissance in military and homeland security applications.**

I. Introduction

Our Stair Climbing Robot (SCR, see Fig. 1) is a small, low-cost Mobile Inverted Pendulum (MIP) robot capable of climbing everyday steps and stairs. Stairs are ubiquitous in human-built environments, and present a specific mobility challenge for (otherwise, highly efficient, fast, coordinated, and robust) wheeled robots. Most robots that climb stairs rely on their size to climb, either by spanning three or more steps at a time, or by having wheels much larger than the step's rise. This paper proposes a simple stair-climbing robot design that leverages feedback control to allow a much smaller/lighter MIP-like vehicle to overcome steps and stairs in human-built environments.

Stair-climbing wheeled robots fall into three main categories: multi-wheeled and treaded vehicles, hopping robots, and dynamic wheeled robots. Multi-wheeled vehicles are the most common and, if large enough, can fairly easily traverse steps. There are many examples of multi-wheeled stair-climbing robots that have passive [3] or active climbing mechanisms [6][5]. However, these designs must be large enough to be able to span at least three steps at once in order to maintain stability.

The second category that has shown some promise is that of jumping robots, which often store energy either mechanically [8][7] or chemically [9][10]. Once this energy is released, such robots can jump very high indeed, sometimes over 60 times its body length [10]. Disadvantages with this approach often include a small number of possible hops and a lack of precise trajectory control once the vehicle is (energetically) launched airborne. Such highly energetic motions are also dangerous to individuals nearby, distinctly unstealthy/loud, and sometimes damaging to the vehicle itself.

[1]emails: {djyang,bewley}@ucsd.edu

Fig. 1: Our patent-pending Stair Climbing Robot prototype.

The third broad category is that of dynamic stair-climbing robots. These are usually wheeled vehicles with additional degrees of freedom [4] that leverage feedback to stabilize quasistatic (usually, slow) stair-climbing maneuvers. We have identified two existing stair-climbing robot designs of this type in the literature: the planetary wheel MIP [1] [2], with a passive differential that shifts the robot's center of mass to climb stairs, and Dean Kamen's patented wheelchair robot design [11], which employs a similar strategy. Both of these designs require the wheels to be larger than the rise of each step (wheel size 508mm, step 120mm), making their robot heavy (17kg) and tall. In comparison, though SCR's leg needs to be larger than that of the rise of the steps it is to overcome, SCR's chassis and wheel dimensions can be selected largely independent of the rise and run of the stairs, allowing more opportunities for miniaturization and robustification, thereby lowering costs and improving safety. In this paper, we describe the several important design considerations for SCR, model its dynamics, optimize design parameters for leg balancing, discuss feedback control methods to stabilize these dynamics, and finally show experimental results for the three key maneuvers necessary for stair climbing with SCR: MIP balancing, leg balancing, and self uprighting.

II. Robot Design

SCR consists of three body components (Fig. 2): the wheels, chassis, and the leg. The wheels are directly mounted to gear motors (with load bearings on the output shafts),

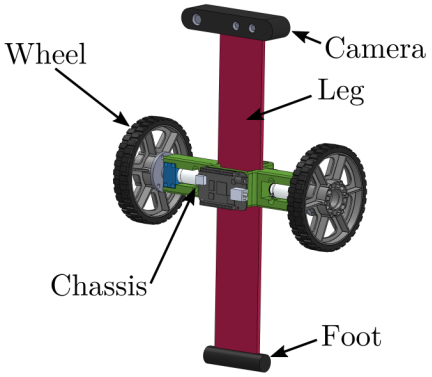

Fig. 2: CAD of SCR. The chassis slides up and down the leg, actuated by a timing belt and gear motor (not shown).

which are mounted on the chassis. The chassis can slide up and down the leg, and is actuated by a timing belt and motor. Note that there are only three motors in this design, two for the wheels and one for driving the leg mechanism.

A. Modes of Operation

SCR has four modes of operation (Fig. 3): (1) **driving**, during which the robot is passively stable, with the leg dragging on the ground (like a Recon Scout), (2) **MIP balancing**, during which the robot drives around balancing on two wheels, with an improved viewpoint for the cameras mounted within the raised "foot", (3) **leg balancing**, during which the robot balances on its lower "foot", using its wheels as reaction wheels to maintain fore/aft balance and its leg motor to raise the chassis up the leg, and (4) **self uprighting**, during which the robot transitions quickly from driving to MIP balancing by applying a strong torque to the wheel motors.

B. Mechanical Design

TABLE I: Motor Parameters

Parameter	Value
No Load Speed	$V_{nl} = 6000rpm$
Stall Torque	$\tau_{stall} = 59.7mNm$
Gear Ratio	$\gamma = 21$
Voltage	$V_{max} = 12V$
Resistance	$R = 3.69\Omega$
Torque Const.	$k = 18.4mNm/A$

The SCR prototype presented here is constructed with mostly 3D-printed plastic. The leg is made of low friction acetal plastic and is constrained to only move up and down by 3D printed sliders. The wheels are directly attached to two brushed Maxon DCX 22mm motors with 21:1 planetary gearboxes. The drive motors' parameters can be found in Table I.

In order to survive repeated falls while leg balancing, the drive motors were soft mounted so that a large bearing could directly transfer radial loads from the hub to the chassis (Fig. 4). The soft mounting also prevents the motor from being over-constrained by the extra bearing.

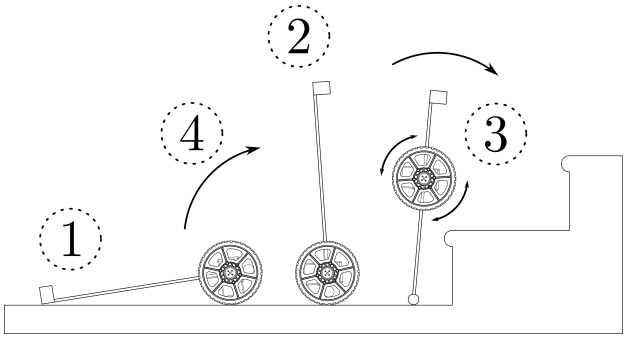

Fig. 3: Four operating modes of SCR: driving (1), MIP balancing (2), leg balancing (3), and self upright (4).

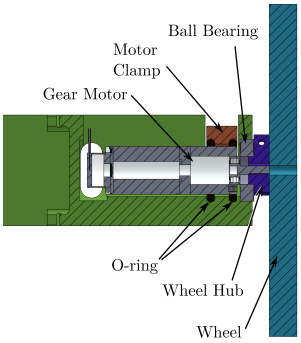

Fig. 4: Cutaway of the soft mounted drivetrain: the gear motor is soft mounted to the chassis with two o-rings and a clamp. The ball bearing is press fit into the chassis the hub is slip fit into the bearing's .5in inner diameter.

The leg is actuated by a high-torque gear motor and a timing belt. The belt is fed through two idler pulleys, and wraps around a timing belt pulley attached to the gear motor. Figure 5 shows details of how the motor actuates the leg. We selected a 43:1 gear motor with stall torque .56Nm and no load speed of 36.6rad/s to actuate the leg. We found this motor to have sufficient torque and speed to lift the chassis along the leg.

For computing the feedback control, the prototype uses

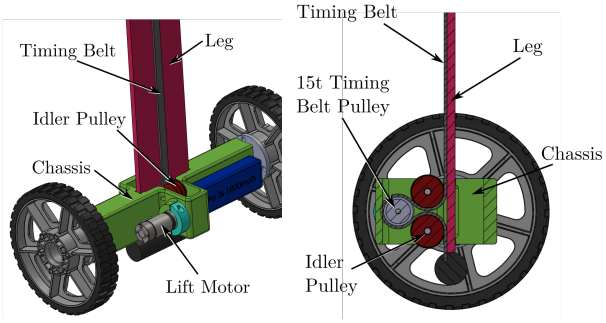

(a) (b)

Fig. 5: Lift mechanism: a) Isometric view b) Section view.

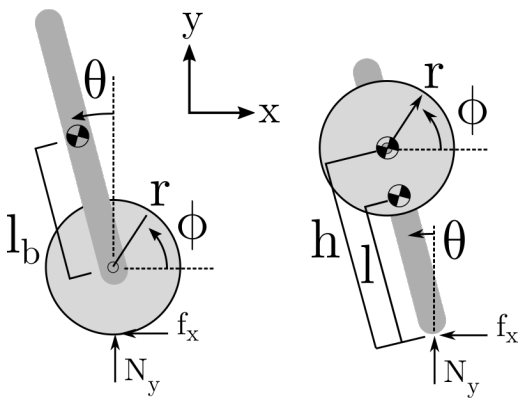

Fig. 6: Coordinate systems for MIP balancing (left) and leg balancing (right).

a BeagleBone Black and the BeagleBoard.org Robotics Cape, which obtains attitude estimates through an Invensense MPU-9250 Inertial Measurement Unit (IMU). The robot obtains wheel and chassis height measurements from encoders mounted on the wheel and lift motors.

TABLE II: Parameters for the SCR prototype in Fig. 1.

Parameter	Variable	Value
leg mass	m_l	$330g$
leg inertia	I_l	$40e^{-4}kgm^2$
leg center of mass	l	$17cm$
chassis mass	m_c	$930g$
chassis inertia	I_c	$4.2e^{-4}kgm^2$
chassis height	h	$varies$
single wheel mass	m_w	$390g$
single wheel inertia	I_w	$2.4e^{-3}kgm^2$
effective wheel inertia	$\hat{I}_w$	$\hat{I}_w = I_w + \gamma^2 I_m$
wheel radius	r	$11cm$
body mass	m_b	$1260g$
body inertia	I_b	$44e^{-4}kgm^2$
body center of mass	l_b	$6cm$

III. Equations of Motion: MIP Balancing

Both leg and MIP balancing share the same nomenclature and similar assumptions. Both systems consist of three connected rigid bodies (leg, chassis, and wheels) with masses and inertias. Referring to Fig. 6, the variables m and I represent the masses and moment of inertias about their body's center of mass. The subscripts l, c, and w represent the leg, chassis, and wheels. l is the distance from the foot's contact point to the leg's center of mass, and h is the position of the chassis along the leg. θ and ϕ represent the body and wheel rotation relative to the lab inertial frame. τ_m represents the motor's torque. Finally, N_y and f_x are the two contact forces with the ground. We simplify the system into a planar 2D system and account for the two wheels and motors by doubling the motor torques and wheel mass properties. A no slip assumption allows the contact friction f_x to be boundless. To derive the equations of motion, we use the free body diagram (Fig. 6) and Lagrangian dynamics to obtain the full planer dynamics as shown in our earlier Ball balancer MIP work [12] [13]. For MIP balancing, we can assume the leg and chassis are a single body, denoted by the subscript b).

$$\left[\hat{I}_w + (m_w + m_b)r^2\right]\ddot{\phi} + m_b r l_b \cos\theta\ddot{\theta} - m_b r l_b \sin\theta\dot{\theta}^2 = -\tau_m \quad (1)$$

$$m_b r l_b \cos\theta\ddot{\phi} + \left[I_b + m_b l_b^2\right]\ddot{\theta} - m_b g l_b \sin\theta = \tau_m \quad (2)$$

Next, we augment the equations of motions with a simplified motor model:

$$\tau_m = k_1 u - k_2\dot{\phi} \quad (3)$$
$$k_1 = kV_{max}/R_m$$
$$k_2 = k^2/R_m$$

where k is the motor constant, V_{max} is the maximum battery voltage, R_m is the motor internal resistance and u is the effective motor duty cycle.

We linearize the dynamics by substituting $\theta = \bar{\theta} + \theta'$, $\phi = \bar{\phi} + \phi'$, and $\tau_m = \bar{\tau}_m + \tau_m{}'$, which are the nominal state (bar) terms and a small perturbation (prime). We take the Taylor series expansion of the trig functions and neglect all the quadratic and higher terms in the perturbations [13]. Setting the nominal conditions $\bar{\theta}$, $\bar{\phi}$, $\bar{\tau}$ equal to zero gives us the resulting linearized dynamic equations:

$$\left[\hat{I}_w + (m_b + m_w)r^2\right]\ddot{\phi} + m_b r l\ddot{\theta} - k_2\dot{\phi} = -k_1 u \quad (4)$$

$$m_b r l\ddot{\phi} + \left[I_b + m_b l^2\right]\ddot{\theta} - m_b g l\theta + k_2\dot{\phi} = k_1 u \quad (5)$$

IV. Equations of Motion: Leg Balancing

The derivation of the leg balancing dynamics are similar, we combine the chassis and leg bodies by assuming that the lifting mechanism is quasistatic and h is not time varying.

$$\left[I_c + I_l + \hat{I}_w + h^2(m_c + m_w) + l^2 m_l\right]\ddot{\theta} - \left[l m_l + h(m_c + m_w)\right] g \sin\theta = -\tau_m \quad (6)$$

$$\hat{I}_w\ddot{\phi} = \tau_m \quad (7)$$

As with MIP balancing, we linearize by taking the Taylor series expansion of the $\sin\theta$ term and augment the model with the motor model (eq. 3) to obtain:

$$\left[I_c + I_l + \hat{I}_w + h^2(m_c + m_w) + l^2 m_l\right]\ddot{\theta} - \left[l m_l + h(m_c + m_w)\right] g\theta - k_2\dot{\phi} = -k_1 u \quad (8)$$

$$\hat{I}_w\ddot{\phi} + k_2\dot{\phi} = k_1 u \quad (9)$$

V. Design Parameter Optimization

The most challenging aspect of SCR's design is determining the mass distribution of the robot. The leg, wheel, and chassis inertias are all significant during the various modes of operation, and impose competing objectives driving this selection. Leg balancing is the most difficult to achieve because the dynamics are heavily coupled between motor

parameters and body and wheel inertias. The bulk of our optimization effort was focused on leg balancing because it is the most challenging, delicate, and interesting. Leg balancing can be readily understood by considering the principle of conservation of angular momentum: applying a torque to the wheels causes the body to rotate in the opposite direction. For the reaction wheels to provide a large torque, they need a significant moment of inertia. From the leg balancing equation 6, we see that to increase the control authority on the body's angle θ, we need to increase the wheel inertia I_w, suggesting the need for a large and heavy reaction wheel. However, the mass of the wheel m_w appears in the body inerta's $h^2(m_c + m_w)$ term. Not only does this term degrade balancing performance, but also it quadratically increases the body's inertia as the height of the chassis increases. The competing design decisions motivated the need for an optimization based approach towards designing the robot. We focused on three design variables: the motor gear ratio, wheel mass, and wheel radius. We did not consider the motor parameters for two reasons: we already had the motors and that the chassis and structure would need to scale accordingly for smaller or larger motors. To gauge the effectiveness of the parameters, we created a open loop computational model which simulated the maximum lean angle the robot can recover. This lean angle was selected as our objective function to be maximized. Table II shows the final mass and inertia distributions of the SCR prototype. These mass distributions, as well as our discussion in this section, can be used as a starting point for future prototype builds.

A. *Parameterized Wheel*

The robot's wheels were 3D printed with steel masses attached to the edge of the wheel to maximize the wheel's inertia (Fig. 10). For our optimization simulation, we parameterize this wheel as a plastic disk with variable radius and mass added to the edge of the wheel. The larger the wheel radius, the more plastic must be used to achieve the size, resulting in lower relative inertia. However, the larger wheels require the robot to raise higher to overcome the stair step. The extra height will drastically decrease the wheel's inertia relative to the body's inertia resulting in a decrease in performance.

B. *Effect of Gear Ratio*

The gear ratio plays an interesting role in leg balancing. The leg balancing problem is a function of available motor torque, which is inversely proportional to wheel speed. If simply considering maximum motor torque, the reaction wheels would be unable to produce torque at moderate wheel speeds. In addition, total effective inertia of the wheel is given by $\hat{I}_w = I_w + \gamma^2 I_m$, where I_m is armature's inertia and γ is the gear ratio. The the gear ratio quadratically increases the motor's effective inertia and makes a significant contribution to the total effective inertia. In our final configuration, the motor's inertia contributes 9.4% of the total wheel inertia. Most importantly, if the motor armature spins in the opposite direction of the wheel, as with the case of a odd number stage gearbox, the reaction torques of the wheels and motor counter each other, which is undesirable.

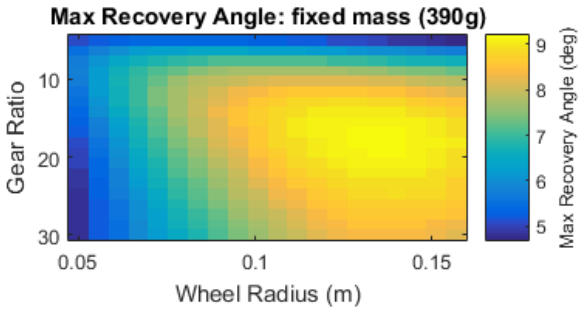

Fig. 7: Given a fixed wheel mass of 390g we can see optimal configuration is a gear ratio of $18.2:1$ and radius of $13.5cm$. However the optimization curve is relatively flat in that region, so there are several configurations that can provide similar performance.

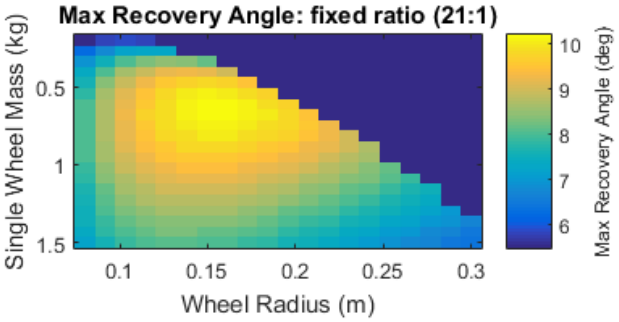

Fig. 8: Given a fixed gear ratio of 21:1 we see that the optimal configuration is wheel of radius $.15m$ and mass $680g$. The dark blue region are configurations that are not physically realizable by our parameterized wheel model (ie, a really large wheel that has very little mass).

C. *Leg Balance Optimization*

In order to find an optimal configuration for leg balancing, we simulated the maximum recovery angle with across an evenly spaced grid ($j = 10$) of gear ratio, wheel radius, and wheel mass at the minimum leg height h to overcome a 20cm step. All other parameters were kept constant: chassis mass, leg mass, (Table II), and motor parameters (Table I). Since there were only three design parameters ($n = 3$) and a coarse grid (resulting in n^j simulations), we were able to use a brute force optimization approach to determine the maximum recovery angle. Two plots of the objective function at fixed wheel mass and fixed gear ratio are shown in Fig. 7 and 8.

To experimentally validate our optimization results, we tested the maximum recovery angle of our robot with varying wheel mass using a 21:1 gear ratio and .11m radius wheel. For every experiment, we started the robot at an initial lean angle, inputted a step input into the motors, and observed whether or not the robot could recover to a vertical position. We increased the initial lean angle until the robot could

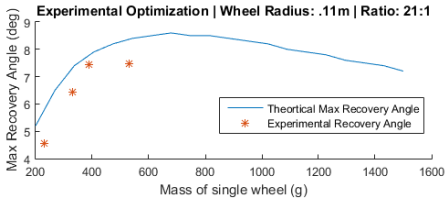

Fig. 9: The maximum lean angle was simulated for varying masses and compared to experimental results. The maximum recovery angle increases as the mass increases up until a certain point. In practice, wheels heavier than 400g put too much physical stress on the robot, causing the leg to bend and vibrate.

Fig. 10: Wheels tested (from left to right): off-the-shelf plastic wheel with urethane tread that was unable to achieve leg balancing. Black 3D printed wheel used for testing with slots to add mass. A red 330g wheel with rubber tread. Through optimization, we arrived at a 390g wheel.

not recover, which is recorded as the maximum recovery angle for that wheel mass. The results of this experiment are show in Fig. 9. Ultimately, the global maximum was deemed impractical ($r = .18m$, $\gamma = 31$, $m = 980g$) since the large mass would put too much structural stress on the mechanical elements and the wheel radaii were as large as a stair step. Regardless, the optimization results guided our final robot parameter selection. The objective functions (Fig. 7, 8) have gentle gradients near their maximums, suggesting a range of values can have similar performance. The final parameters were selected by weighing the simulated results with practical considerations. In the future, a comprehensive optimization should be done with additional design variables such as: motor parameters, structural reinforcement, lift motor speed, and energy consumption.

VI. Controls

A. MIP Balancing Controls

In order to achieve MIP balancing, we must control the wheel rotation $\phi(t)$ and the body angle $\theta(t)$ with only one input, $u(t)$ making it a SIMO (single-input, multiple-output) dynamic system. To accomplish this, we leverage a linear-quadratic regulator (LQR) to control the system. Our system states are given as $x = [\dot{\theta}, \theta, \dot{\phi}, \phi]^T$. We apply Bryson's rule to obtain $Q = diag(.1, 1, .1, 1)$ and $R = 1$ to prioritize the absolution body and wheel position over their velocities. The final gains used were

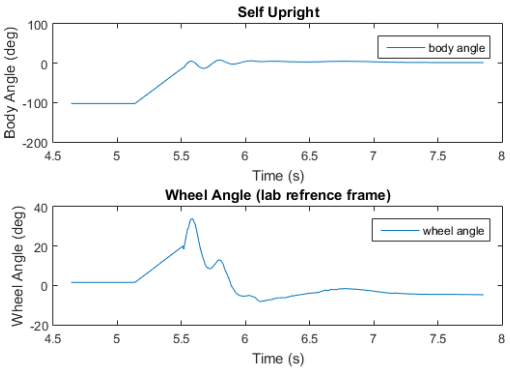

Fig. 11: Self upright maneuver and MIP balancing. The robot begins with the leg dragging on the ground. A bang-bang controller is used to self uprighted the robot within 7cm.

$K = [-0.9891, -.014142, -0.1679, -0.0265]$. We found these gains to give adequately stabilize the MIP about it's equilibrium point.

B. Leg Balancing Controls

In order to achieve leg balancing we need to control the body angle θ to prevent the motors from saturating by minimize the wheel speed $\dot{\phi}$. This SIMO Leg balancing system was also stabilized using LQR control (eq. 10). Our system states are given as $x = [\dot{\theta}, \theta, \dot{\phi}]^T$. We priortized the body angle more than the wheel speed by choosing $Q = diag(1, 1, .01)$ and $R = 1$. Minor hand tuning on the wheel velocity $\dot{\phi}$ gains were needed to prevent the robot from responding too aggressively to the encoder's discretization noise at low velocities.

$$u(t) = k_{\dot{\theta}}(\dot{\theta}_{ref} - \dot{\theta}) + k_{\theta}(\theta_{ref} - \theta) + k_{\phi}(\dot{\phi}_{ref} - \dot{\phi}) \quad (10)$$

To balance the robot as the chassis rose up the leg, we linearly interpolated between the maximum and minimum height controllers. Since the controller gains are generated LQR, we can easily obtain different gains for the varying chassis heights. The gain scheduling approach is shown in equation 11. Two exceptions were made: we kept $k_{\dot{\phi}}$ constant because the optimal gains varied by less than 5%, and we caped the k_{θ} gain for chassis heights above .24m because the controller was too physically aggressive for our system.

$$k_{\dot{\theta}}(h) = -4.499h - 0.1331 \quad (11)$$
$$k_{\theta}(h) = -21.0226h - 3.5741 \quad (12)$$
$$k_{\phi}(h) = -0.0217 \quad (13)$$

VII. Experimental Results

Through design parameter optimization and optimal control, we were able to determine effective mass distributions and controllers and to achieve MIP balancing, leg balancing, and self uprighting.

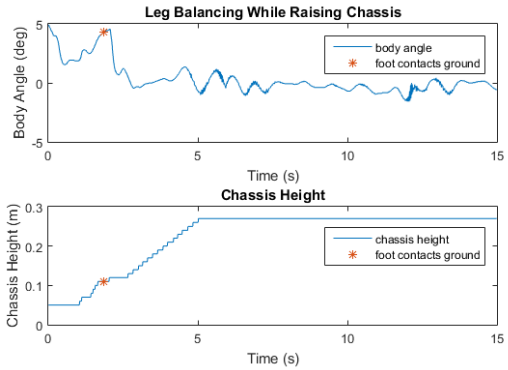

Fig. 12: The robot was commanded to leg balance while the chassis raised to .26m over 5 seconds. Gain scheduling was used to balance the robot at changing leg heights.

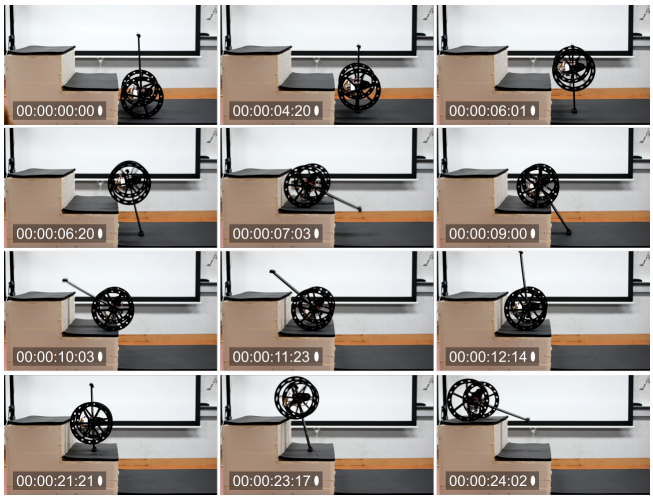

Fig. 13: Screen captures of SCR climbing up two steps. At t=0 and 12s, the robot is MIP balancing. At t=4, 6, 21s the robot is Leg Balancing. At t=6.2, 23s SCR is falling onto the step. Finally at t=9, 10, 11s SCR pulls the leg through the body and self upright.

Figure 11 shows the self uprighting maneuver followed by MIP balancing. Self uprighting was robustly achieved with a simple bang-bang controller in less than 10cm of travel.

In leg balancing mode, the robot could balance indefinitely at chassis heights below .26m. Balancing at greater heights was possible for several seconds due to the quadratically increasing body inertia. Figure 11 shows the robot transition between MIP balancing and leg balancing at .26m. Overall the performance of the three key modes of operation for SCR to climb stairs were adequate climb up steps with rise .20m and run .28m via open loop commands (Fig.13). The fastest the robot could safely climb steps was 10 seconds per step, but there is certainly room for improvement.

VIII. Conclusions and Future Work

This paper presents the design and control of a prototype SCR design. This robot represents a new class of small, lightweight robots capable of slowly and steadily climbing stairs. We identify the importance of optimizing the mass and inertia properties of the vehicle and presented the competing objectives driving this design through both simulation and experimentation. Finally, we were able demonstrate our SCR prototype for the three key maneuvers: MIP balancing, leg balancing, and self uprighting and showed the ability of the robot to climb stairs.

Based our initial prototype, we can now refine and further optimize our design. The choice of the 22mm maxon motor was simply because this was the motor initially selected for the project. After the optimization results, we realized that a smaller, less powerful motor could achieve better leg balancing performance. Smaller, lighter motors would lead to a cascade of weight reduction: less structural reinforcement, smaller battery, and smaller lift motor. By decreasing the chassis mass, the reaction wheels will be much more effective. In order to develop a truly optimal SCR design, we suggest considering additional design variables in the optimization such as motor size and a parameterized chassis model that scales with the size and forces that the robot must endure. Finally, in order to achieve quick and robust stair climbing we plan to employ computer vision to estimate the rise and run of a staircase, and the robot pose in front of it, in order to climb stairs autonomously.

References

[1] Takaki, Takeshi, Tadayoshi Aoyama, and Idaku Ishii. "Development of inverted pendulum robot capable of climbing stairs using planetary wheel mechanism." *Robotics and Automation (ICRA), 2013 IEEE International Conference on. IEEE*, 2013.

[2] Wardana, Ananta Adhi, et al. "Development of a control system for a stair-climbing inverted pendulum robot." *Instrumentation, Control and Automation (ICA), 2016 International Conference on. IEEE*, 2016.

[3] Turlapati, Sri Harsha, et al. "Stair climbing using a compliant modular robot." *Intelligent Robots and Systems (IROS), 2015 IEEE/RSJ International Conference on. IEEE*, 2015.

[4] Foo, Edwin, and Thanh Tung Le. "STARCLY robotA novel compact stair climbing robot." *Mechanical and Electronics Engineering (ICMEE)*, 2010 2nd International Conference on. Vol. 2. IEEE, 2010.

[5] Mihankhah, Ehsan, et al. "Autonomous staircase detection and stair climbing for a tracked mobile robot using fuzzy controller." *Robotics and Biomimetics*, 2008. ROBIO 2008. IEEE International Conference on. IEEE, 2009.

[6] Matthies, Larry, et al. "A portable, autonomous, urban reconnaissance robot." *Robotics and Autonomous Systems* 40.2 (2002): 163-172.

[7] Schmidt-Wetekam, Chris, et al. "Design, optimization, and control of a new class of reconfigurable hopping rovers." *Decision and Control, 2007 46th IEEE Conference on. IEEE*, 2007.

[8] Woodward, Matthew A., and Metin Sitti. "Design of a miniature integrated multi-modal jumping and gliding robot." *Intelligent Robots and Systems (IROS), 2011 IEEE/RSJ International Conference on. IEEE*, 2011.

[9] Tolley, Michael T., et al. "An untethered jumping soft robot." *Intelligent Robots and Systems (IROS 2014), 2014 IEEE/RSJ International Conference on. IEEE*, 2014.

[10] Ackerman, E. "Boston dynamics sand flea robot demonstrates astonishing jumping skills." *IEEE Spectrum Robotics Blog 2.1* (2012).

[11] Kamen, Dean L., Robert R. Ambrogi, and Richard Kurt Heinzmann. *"Transportation vehicles with stability enhancement using CG modification."* U.S. Patent No. 5,975,225. 2 Nov. 1999.

[12] Yang, Daniel, et al. "Design and control of a micro ball-balancing robot (MBBR) with orthogonal midlatitude omniwheel placement." *Intelligent Robots and Systems (IROS), 2015 IEEE/RSJ International Conference on. IEEE*, 2015.

[13] T. Bewley, "Numerical Renaissance: simulation, optimization, and control," 2017, Renaissance Press.